

Cyclic perturbations facilitate athermal creep in yield-stress materials†

Cite this: DOI: 10.1039/d5sm00186b

 Ezequiel E. Ferrero *^a and Eduardo A. Jagla ^b

Yield stress materials deform irreversibly at a finite strain-rate if loaded with a fixed stress σ larger than some critical yield stress σ_c . When $\sigma < \sigma_c$ deformation is absent, except for transient or thermally activated processes. However, the cyclic temporal variation of system parameters can induce a persistent irreversible deformation under sub-critical athermal conditions. We characterize this phenomenon using well established models in the fields of the yielding and depinning transitions. We find that the amount of deformation per cycle increases if σ_c is approached from below, and it decreases and even vanishes at a novel critical stress $\sigma_0 < \sigma_c$ when this is reached from above. Interestingly, σ_0 plays a role similar to the fatigue limit in the context of fatigue damage propagation. Our study is inspired by the literature on soft Earth geophysics where soil creep mechanisms have been correlated with cyclic changes of environmental conditions, such as daily or seasonal fluctuations in temperature and humidity, which in turn promote fluctuations in the systems internal mechanical properties. We believe our findings can motivate an interdisciplinary perspective on the study of sub-critical landform evolution, as the creep of hill slopes over long periods of time.

 Received 21st February 2025,
Accepted 18th June 2025

DOI: 10.1039/d5sm00186b

rsc.li/soft-matter-journal

I. Introduction

There is a renewed interest in the study of the ‘thin skin’ of the Earth.^{1,2} The understanding of the soft matter landscape on which we live comes up as increasingly essential in times of climate change. Several hazardous events, such as landslides, earthquakes, faulting, and ice fractures, are related to the slow evolution of landscapes. In particular, well-known evidence indicates that terrains systematically evolve downhill over long periods of time (years and beyond), a phenomenon known as soil creep in geophysics.^{3,4} This sub-critical crawling motion exhibits dynamics similar to that of yield-stress materials. These are systems encompassing gels, foams, emulsions and polymeric, colloidal and granular glasses, characterized by a macroscopic persistent deformation rate if applied stress σ is larger than some critical value σ_c .^{5,6} This analogy has motivated the study of geophysical problems with tools and models inherited from condensed matter and statistical physics, on a field now called soft Earth geophysics.^{1,2}

Under sub-critical conditions ($\sigma < \sigma_c$) the deformation of amorphous materials can be either a transient effect (usually

referred to as ‘Andrade creep’)^{5–9} or a thermally activated flow,^{10,11} which eventually at very small driving is analogous to the thermal creep of elastic interfaces in random media.^{12–14} In soils (a case of granular matter composed by sand, rocks, clay, organic remains, *etc.*), it is quite clear that thermally activated processes are almost negligible, and the possibility of long lasting but transient deformations is under debate. For instance, recent experiments on sand-piles,^{15,16} essentially an athermal system, have shown sustained creep motion at sub-critical slopes in undisturbed setups, and presented these “quenched quiescent heaps that creep indefinitely” as a challenge to granular rheology. This raises a natural question: what other sub-critical flow mechanisms, aside from transient or thermally activated creep, should be considered in soft Earth geophysics?

Unlike typical soft matter systems studied under controlled laboratory conditions, soils experience various mechanical perturbations that, along with gravity, can contribute to sub-critical flow.^{17–19} They include vibrations caused by walking of animals, vegetation movement due to wind, water falling and flow during rain, and even earthquakes. To some extent, all of them have the potential to produce a persistent down hill evolution of the soil.^{20–24} Other relevant source of external perturbations comprise those originated by periodic variations of parameters through changes of environmental conditions that affect the internal properties of the system. Key examples include daily or seasonal variations in temperature and humidity, which microscopically alter the size, surface properties, and mechanical response of soil constituents, thereby affecting the internal interactions and evolution of the system. The effect of

^a Instituto de Nanociencia y Nanotecnología, CNEA-CONICET, Centro Atómico Bariloche, (R8402AGP) San Carlos de Bariloche, Río Negro Argentina. E-mail: ezequiel.ferrero@conicet.gov.ar

^b Centro Atómico Bariloche, Instituto Balseiro, Comisión Nacional de Energía Atómica, CNEA, CONICET, UNCuyo, Av. E. Bustillo 9500 (R8402AGP) San Carlos de Bariloche, Río Negro, Argentina

† Electronic supplementary information (ESI) available. See DOI: <https://doi.org/10.1039/d5sm00186b>

cyclic variation of temperature has also been studied in other contexts. Notably, in metallic glasses²⁵ it was found that thermal cycling, even when well below the glass temperature of the material, induces rejuvenation. So, although no macroscopic flow is observed, plastic rearrangements occur, likely associated to the mechanical thermal expansion and contraction. In granular systems, thermal cycling effects (sometimes referred to as thermo-mechanical ratcheting) have also been under scrutiny in the last years,^{26–32} primarily by the mechanical engineering community. Overall, there is qualitative agreement that oscillatory changes in environmental conditions can significantly affect the dynamic evolution of the system. In the case of a sloped terrain, this may lead to a persistent downhill displacement. This phenomenon is the focus of the present manuscript, where we mainly engage with models and ideas from driven phase transitions in disordered systems.

The first report of the phenomenon of downhill movement under oscillatory external conditions is most likely that of Moseley³³ in his letter ‘on the descent of glaciers’ (1856). He analyzed the case of a slab of material resting on an inclined plane due to frictional contact. Under periodic variations of temperature, the slab expands and contracts, and a simple mechanical analysis predicts that on each full variation cycle there is a net descent of the slab. His idea was criticized at that time for being over-simplistic. Nevertheless, it describes the essential phenomenology that is present in more complex and realistic systems. Moseley’s idea was recapitulated more recently by Croll,³⁴ who discussed with illustrative examples of ice-rich materials and asphalt pavements that, when a solid is subject to alternations of tension and compression (following alternations in temperature), some motion can be produced even in situations where gravity is either absent or, further, against the prospective motions. Blanc, Pugnali and Géminard³⁵ have applied the analysis of Moseley to a numerically-simulated one dimensional chain of blocks connected through elastic springs that rest on an incline. Introducing a cyclic variation of the rest length of the springs (mimicking a thermal expansion-contraction of a macroscopic material) they observed a reptation of the chain down-hill and were able to estimate its average creep velocity. They used a phenomenological Amontons–Coulomb friction law between blocks and the substrate. Additionally, the absence of stochastic elements in their model led to a behavior reminiscent of ideal dynamical systems, such as peculiar synchronizations, limit cycles, and plateaus in the dynamical evolution. Although with limitations, these previous works already gave a qualitative idea of the phenomenon we will discuss: a sub-critical flow based on the periodic variation of inter-element interactions that we can ascribe in real systems to changes in environmental conditions.

Our approach introduces some elements that bring these ideas closer to the effective description of the concrete phenomenon of soil creep. First of all, we do not introduce any *ad hoc* form for a friction law. Instead, we consider the overdamped evolution of a system of mesoscopic ‘blocks’ or regions of an amorphous material, and eventually the appearance of a friction-like law (*viz.*, depinning/yielding) is an emergent property in our treatment. Our model incorporates a degree of

randomness, coded mainly in the stochastic form of the interaction/deformation potentials, and this smooths out the synchronization effects that might appear in the absence of such a randomness. Finally and most importantly, we do not limit to the description of a frictional situation between two solid bodies, neither to zero- or one-dimensional systems. In fact, we consider here two-dimensional systems of two families of problems: (i) depinning models, typically used to describe the driven transition between rest and motion of an elastic manifold driven on top of a disordered pinning potential, and (ii) yielding models, typically used to describe the bulk deformation of an homogeneous amorphous material under an applied external shear stress.

In particular, the implementation of the yielding case is suited to describe the slow deformation of a bulk material, which is the case that is most relevant to describe the soil creep phenomenon. As a matter of fact, ‘Eshelby’-like correlations in the strain field, a distinctive characteristics of the yielding models, have been reported in granular heaps experiments recently.¹⁶ Therefore, returning to our inspiration from soft Earth geophysics problems,^{1,15,16} we believe that the kind of sub-critical deformation mechanism that we analyze, its underlying mechanisms and universal features, can be further explored and extended to tackle concrete examples in that field.

To provide insights in the basic underlying phenomenology, we first present in Section II the simple example of a two-particle system joined by a spring that changes its stiffness in a periodic way. Then, we introduce our modeling framework (Section III) and study the oscillatory creep phenomenology in two spatially extended two-dimensional models: (i) an elastoplastic model of amorphous solids, with long-range elastic interactions in Sections IV, and (ii) a driven elastic interface with short range elastic interactions, in Section V. In Section VII, we wrap up these findings considering a fully-interacting mean-field system where some analytical results can be obtained. Finally, we present our conclusions and pose some additional questions in Section IX. The article also includes three appendices. Appendix A contains some details about the simulation methods and protocol for completeness and reproducibility. In Appendix B we discuss the use of different disorder types in a fully-connected model. In Appendix C we derive the analytic results of the mean-field model presented in Section VII.

II. Reptation of a two-particle system caused by oscillation of the interaction intensity

We analyze an elementary system that qualitatively displays the essence of the physical process under study.³⁵ Let us consider two particles of mass m joined by a spring, lying on a slope. For a fixed value of the spring constant k , the system may be at rest, or smoothly sliding depending on the value of the slope angle, and the critical friction forces of the particles. Assuming there is some asymmetry between the particles such that the friction

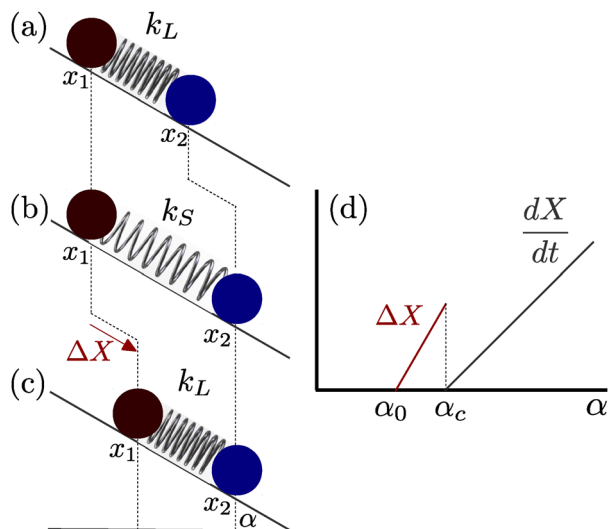


Fig. 1 Schematics of the reptation process by cyclic variations in the interaction forces: two particles linked by a spring of strength k rest on an inclined. For constant k the system behaves according to the black line in (d) that shows displacement rate dX/dt vs. incline angle α , α_c being the minimum slope for system movement. If $\alpha < \alpha_c$, the system performs a reptation upon changing the value of k between k_L and k_S , advancing a distance ΔX on each cycle (a)–(c). There is a minimum slope α_0 for this process to occur.

forces³⁶ are f_1 and $f_2 \neq f_1$, the critical angle α_c for smooth descent at constant velocity is obtained as

$$\sin(\alpha_c) \equiv \frac{f_1 + f_2}{2mg}. \quad (1)$$

Note that α_c is independent on the value of k .

If $\alpha < \alpha_c$ we could expect that the system remains always at the same location. However, if the value of k fluctuates (let's say k oscillates between a large value $k = k_L$ and a small value $k = k_S$) and if α is sufficiently close to (but lower than) α_c , then there is an alternate advance of x_1 and x_2 as k passes from k_L to k_S , and back to k_L . This is schematically plotted in Fig. 1. ΔX is the net advance of the system per cycle.

The origin of this reptation phenomenon is the following. Starting from the configuration in Fig. 1(a) with $k = k_L$, the reduction of k to k_S produces an increase of the force on the right-most particle, which moves to the right until it experiences a force equal to its critical force; this is the configuration in Fig. 1(b). Now, as k is increased back to k_L , it is the left-most particle that receives a force larger than its critical one, and moves to the right until the force does not exceed the critical value any more (Fig. 1(c)). A simple calculation shows that $\Delta X = 0$ below a critical angle α_0 given by (we assume $f_1 > f_2$)

$$\sin(\alpha_0) = \frac{k_L f_1 + k_S f_2}{mg(k_L + k_S)}. \quad (2)$$

If $\alpha_0 < \alpha < \alpha_c$ the value of ΔX is given by

$$\Delta X = -\frac{f_1}{k_S} - \frac{f_2}{k_L} + mg \left(\frac{1}{k_L} + \frac{1}{k_S} \right) \sin(\alpha) \quad (3)$$

which is indicated in blue in Fig. 1. This is the phenomenon we discuss in the rest of the paper, distilled to its simplest form.

III. Theoretical framework and modeling

We use a common framework for depinning and yielding phenomena, that of elastic manifolds evolving onto disordered energy landscapes.^{11,37–39} The manifold can either represent an elastic interface $x(\mathbf{r})$ that undergoes a depinning transition, or it can represent the local strains configuration $\gamma(\mathbf{x})$ of an amorphous material (in this case the energy landscape represents the possibility of many different locally stable configurations). We limit ourselves to the study of two-dimensional systems of depinning and yielding in this work. We use short-range elasticity for the depinning case and a long-range (Eshelby-like) elastic propagator for the yielding case.

To fix ideas, let us first describe the case of the depinning of the elastic interface and then declare the analogous quantities for yielding. Apart from the elastic interactions and the forces induced by the underlying disorder potential, the system is subject to an external drive: we note this forcing as f . We consider the local position $x(\mathbf{r}, t)$ of an interface, that we will discretize on a square lattice (with periodic boundary conditions) and denote x_i the position at site i . The temporal evolution of x_i follows an overdamped dynamical equation of the form

$$\frac{\partial x_i}{\partial t} = -\frac{dV_i}{dx_i} + \sum_{(j,i)} k(x_j - x_i) + f \quad (4)$$

where (j, i) in the elastic term indicates nearest neighbor sites. The V_i are quenched disordered potentials that we describe below.

The phenomenology of systems described by eqn (4) is the following. There is a critical value f_c , such that for $f \leq f_c$ the system eventually reaches a stable configuration and stops evolving in time; while for $f > f_c$ it keeps evolving in a finite steady velocity situation. Above and near f_c the velocity v of the elastic interface has a dependence on f of the form $v \sim (f - f_c)^\beta$. The transition at f_c is referred to as depinning,^{40,41} and it is sharply defined only in the ideal case in which other external disturbances are assumed to be negligible. For instance, the presence of a finite temperature produces stochastic fluctuating forces on the elementary constituents in the system that are known to smooth out the transition, turning it into a crossover.^{42–44} This produces thermally activated creep even at very small driving forces.^{12,14,45}

In the present work, while we stick to the athermal case, we incorporate periodic variations of the value of the elastic interactions in the system, generically denoted by k , that will produce a crawling effect on the system and a persistent evolution, as long as the strength of the elastic interactions continue to oscillate. Let us recall that, for a given amplitude of the disorder potential and a fix strength k of the elastic interactions, the critical force f_c depends on k . If for a value of $k = k_1$ we have a critical force f_{c_1} , for $k = k_2 < k_1$ the critical force will be $f_{c_2} > f_{c_1}$. This is because a softer elasticity allows

the interface to better adapt to the disorder potential, occupying deeper local energy minima, and therefore increasing the threshold force needed for depinning. Now we consider what happens if the value of k is cycled between a large value k_L and a small value k_S . Such oscillations in k will produce a minor effect in the moving phase, $f > f_{c,k_S} > f_{c,k_L}$, since the system is already evolving at a finite velocity regardless the value of k . The most surprising consequences of an oscillation in k occur in the fully sub-critical phase $f < f_{c,k_L} < f_{c,k_S}$. Naively one could expect no movement at all in this regime. However, as in the problem analyzed by Moseley,³³ the oscillatory variation of k induces a systematic advance of the elastic manifold that is synchronized with the cycles of the perturbation.

In the steady state, after many oscillation cycles of k , an advance equal to $M\Delta X$ will be observed, where M is the number of cycles applied and ΔX is the advance per cycle. Even though it might be incorrect to talk about a finite velocity of advance, ΔX is a clearly measurable quantity and happens to be non-zero in a non-negligible range of sub-critical forces. ΔX is particularly large when f is only slightly below the critical force $f_c = f_{c,k_L}$, and is shown to decrease as we depart from it. Furthermore, we are able to show that this athermal reptation assisted by the cyclic variation of parameters cannot happen below a minimal external force f_0 , with f_0 depending on k_L and k_S . The above dynamical scenario is schematically illustrated in Fig. 2.

When addressing the case of the yielding transition of driven amorphous solids, we can do a complete analogy of the phenomenology described above for depinning. An amorphous solid subject to an external stress σ will flow in the steady state if $\sigma > \sigma_c$.⁴⁶ In this case, the order parameter of the transition is the deformation velocity or strain-rate $\dot{\gamma}$ that departs from zero as $\dot{\gamma} \sim (\sigma - \sigma_c)^\beta$, typically with $\beta > 1$. We describe a two-dimensional material with periodic boundary conditions. The equation of motion that we solve for each site i is now

$$\frac{\partial \gamma_i}{\partial t} = -\frac{dV_i}{d\gamma_i} + \sum_j G_{ij}\gamma_j + \sigma \quad (5)$$

where the interaction kernel G_{ij} (the sum runs over all $j \neq i$) is chosen to be the Eshelby propagator with an amplitude that we control with a factor k ,

$$G_{ij} \propto k \frac{\cos(4\theta_{ij})}{r_{ij}^2}. \quad (6)$$

Notice that this kernel is long-ranged (details of the implementation can be found in Appendix A). In the case of the amorphous solid, ΔX corresponds to a change in plastic strain ($\Delta X \equiv \Delta\gamma$) instead of interface position. As the depinning counterpart, the yielding transition also displays a thermal rounding phenomenon when temperature is relevant,^{10,11} but we stay in the athermal case in the present work.

The athermal reptation mechanism we are discussing only occurs at driving below and sufficiently close to f_c . Yet the effect may be relevant as many systems are expected to adjust spontaneously into such a condition. For instance, the rest slope of a terrain usually accommodates at an angle just below

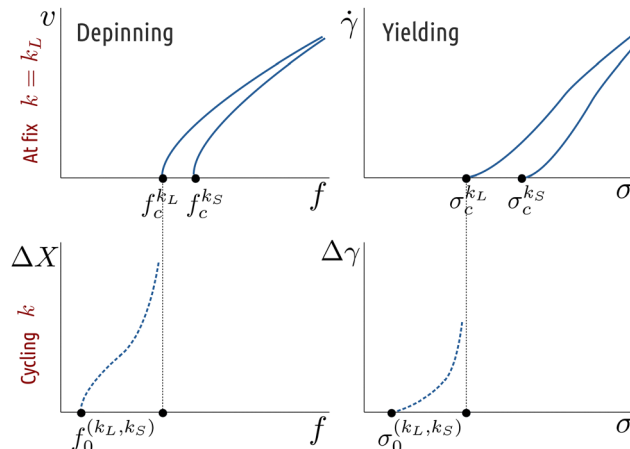


Fig. 2 Schematic display of the crawling mechanism by cyclic variation of parameter k discussed in this work. By oscillating the elastic constant k between k_L and $k_S < k_L$ finite displacements per unit cycle ΔX are obtained at forces which are below both $f_c^{k_L}$ and $f_c^{k_S}$, the depinning forces of the system at fix $k = k_L$ and $k = k_S$, respectively. The same happens in the case of the yielding model with stress σ taking the place of f , an increase per $\Delta\gamma$ is observed. The schematics emphasizes the different forms of the flow-curves for depinning and yielding, and anticipates that this form is reproduced in the behavior of ΔX ($\Delta\gamma$) near f_0 (σ_0).

the rest angle, as it occurs also with a heap of sand or gravel. This is, the system steps at the situation in which the effect of periodic disturbances in the interactions is expected to be maximized.

In most of this study the disordered potentials V_i are chosen to be an alternate sequence of parabolic ‘traps’ and flat regions, as schematically shown in Fig. 14 of Appendix A. For simplicity we have chosen the traps to be identical and to encode the stochasticity in the length of the flat regions of $V(x)$. The use of some stochastic element in the definition of the potentials V_i is rooted in the general framework of depinning and yielding transitions. Beyond this fact, all qualitative results are expected to be independent of the kind of randomness used. We have checked that other forms of the random potentials give qualitative the same results, the main reason for the present choice is that it maximizes somehow the stress range in which the reptation is observed (see also Appendix B for results with a different form of the disorder).

IV. Results for amorphous solids

We first present the results for the yielding model. We numerically solve the equations of motion (5) for different values of the applied stress σ and either fix or oscillating values of k . Details of the implementations can be found in Appendix A.

First, we characterize the system at fixed values of the elastic interaction intensity k , by constructing the corresponding flowcurves for different values of k , Fig. 3. This is done starting at a large value of σ , and calculating the average value of $\dot{\gamma}$ after reaching a steady state along the simulation. Then, σ is progressively reduced in discrete steps and the corresponding values of $\dot{\gamma}$ in a steady state are obtained. We plot $\dot{\gamma}$ as a function

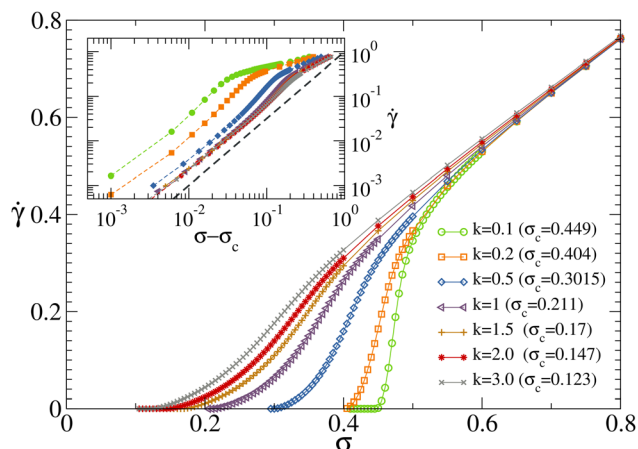


Fig. 3 Yielding model. Flowcurves (strain-rate $\dot{\gamma}$ vs. stress σ) for the 2D elasto-plastic model of an amorphous solid under shear, at different values of the long-range elastic interaction intensity k . The inset shows $\dot{\gamma}$ vs. $\sigma - \sigma_c$, where $\sigma_c = \sigma_c(k)$ depends on k . The dashed line displays a law $\dot{\gamma} \sim (\sigma - \sigma_c)^{1.5}$. Data corresponds to a system of size $N = 1024 \times 1024$.

of σ and this describes a singular law $\dot{\gamma} \sim (\sigma - \sigma_c)^\beta$. This is fully equivalent to the Hershel–Bulkley law in the rheology of complex systems, by just swapping the axes and representing σ as a function of $\dot{\gamma}$, $\sigma = \sigma_c + A\dot{\gamma}^n$, with $n = 1/\beta$, see for instance ref. 6 and 47. We observe in Fig. 3 how the critical stress σ_c depends on k , and increases as k is reduced. Yet, near σ_c all curves behave as $(\sigma - \sigma_c)^\beta$ with $\beta \simeq 1.5$, as it is shown in Fig. 3's inset. This is a well known result of the yielding transition, and the observed exponent β is the one expected in two-dimensions for the ‘cuspy’ type of potential used here.^{37,47} Notice that a smooth potential (or equivalently, a progressive local yielding rule) would give instead $\beta = 2$, which occasionally happens to compare better with experimental measurements^{5,47} and with the $n = 0.5$ yielded by the classic Hébraud–Lequeux mean field approach.^{48,49} It's worth mentioning that, for each value of k , the numerical value of σ_c is non-universal, it has sample to sample fluctuations and also suffers from finite size effects.⁵⁰

In the presence of an applied constant stress below the critical value, we cycle the values of k between the starting large value k_L and a small value k_S . Having the soil creep phenomenon in mind, this cycling is done very slowly, ensuring that a further reduction of the cycling rate does not affect substantially the results obtained (in case of using a more rapid oscillation of parameters the qualitative phenomenon persists, although its quantitative extent is reduced, see Appendix A). We measure the advance $\Delta\gamma$ of the average strain in the system per cycle. The results are presented in Fig. 4. There is a finite range of sub-critical stresses between σ_c and down to some value σ_0 , in which $\Delta\gamma$ is finite. For a fix k_L , as it is the case of Fig. 4, the value of σ_0 depends on k_S . As a matter of fact, the range $\sigma_0 - \sigma_c$ where oscillations produce a non-zero displacement $\Delta\gamma$ becomes wider as $k_L - k_S$ increases. Let us mention that, as σ_c , σ_0 might also suffer from finite-size effects, but these are negligible compared to the gap $\sigma_c - \sigma_0$ which remains finite in the thermodynamic limit as far as $k_S < k_L$. Note also

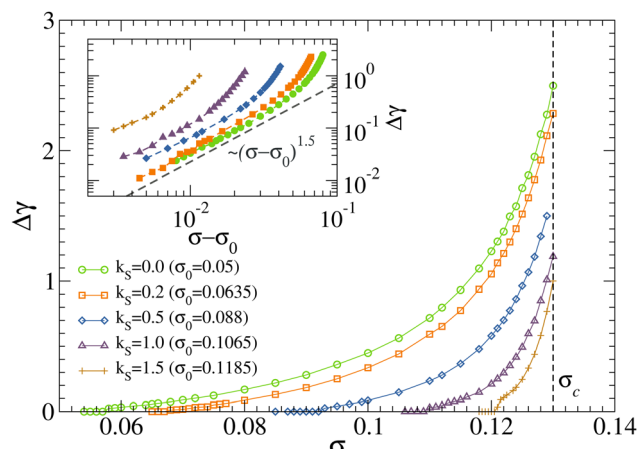


Fig. 4 Yielding model. Strain advance $\Delta\gamma$ vs. stress σ for our 2D elasto-plastic model when cycling between a fixed $k_L = 3.0$ and different values of k_S . The inset displays $\Delta\gamma$ vs. $\sigma - \sigma_0(k_S)$. The power-law $\sim (\sigma - \sigma_0)^{1.5}$ is displayed as guide to the eye. Data corresponds to a system of size $N = 128 \times 128$.

that, independently of the oscillation amplitude, $\Delta\gamma$ increases when approaching σ_c .

Looking at the inset of Fig. 4, we can further point out that the form of $\Delta\sigma$ close to σ_0 is reminiscent of the flowcurves at fix k , this is, it reaches σ_0 with a power-law consistent with $\Delta\sigma \sim (\sigma - \sigma_0)^{3/2}$. We will come back to discuss this similarity in Section VI. Yet, let us advance here that whatever the critical exponent β is around σ_c , according to each known case,⁴⁷ we expect the same exponent to be observed around σ_0 in the oscillatory k athermal creep protocol.

The dependence of σ_c and σ_0 with k_L for different values of k_0 is presented in Fig. 5. The value of $\eta \equiv (\sigma_c - \sigma_0)/\sigma_c$ is a measure of the relative range in which we observe sub-critical flow. We see that η is maximal for $k_S = 0$, and it progressively shrinks as k_S is increased at a fixed k_L . In addition, for a fixed value of k_S the value of η is larger at larger values of k_L , and it decreases as k_L does. The mean field analysis of Section VII suggests that η is different from zero in all the range $k_L > k_S$, yet it is very small when $k_L \gtrsim k_S$.

V. Results for elastic interfaces

We now present results for the effects of changing or oscillating the elastic interaction strength in the case of elastic manifolds on disordered media that undergo a depinning transition. We proceed in analogy with the yielding case described in the previous section, now working with eqn (4).

We characterize the system at fixed values of k , by constructing the corresponding flowcurves, as displayed in Fig. 6. Note how the critical force f_c increases as k is reduced. Still, near f_c all curves behave as $(f - f_c)^\beta$ with $\beta \simeq 0.67$, as it is shown in the inset. A value of β smaller than 1 is a well known characteristic of depinning models, and it is an important difference with the yielding case, where $\beta > 1$. Moreover, we observe compatibility with the exponent expected for short-range depinning in $d = 2$.^{13,51}

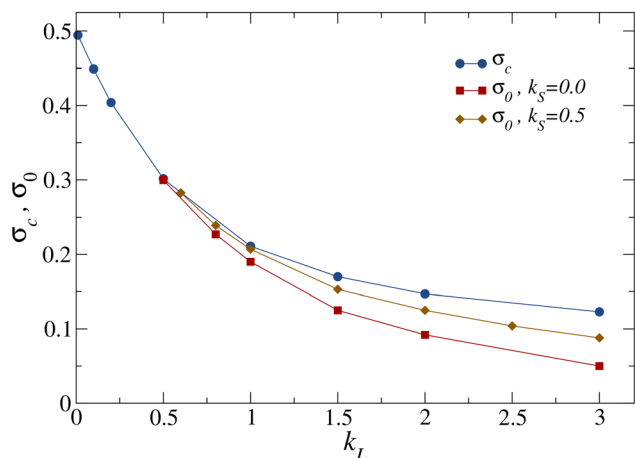


Fig. 5 Yielding model. Yielding critical stress σ_c (blue circles) and σ_0 (red squares for $k_S = 0$, chocolate diamonds for $k_S = 0.5$) vs. k_L . System sizes used are $N = 1024^2$ and $N = 128^2$ for the curves of σ_c and σ_0 , respectively.

In the presence of an applied force smaller than the critical one, we cycle the values of k between the starting value k_L and the a final value k_S . As in the yielding case, we observe an advance ΔX per cycle of the interface; results are presented in Fig. 7. There is a finite range of forces between some f_0 and the critical force f_c , in which the value of ΔX is finite. Note how ΔX increases when approaching f_c . The range $[f_0, f_c]$ where the effect is observed becomes wider as $k_L - k_S$ increases. Since we work in Fig. 7 at a fixed $k_L = 0.2$, the range of forces at which the subcritical athermal reptation occurs is maximal for $k_S = 0$. Again, as in the yielding case, we point out that the form of ΔX close to f_0 seems to be consistent with a ‘shift’ of the criticality from f_c to f_0 , *i.e.*, ΔX maintains the $\beta \simeq 2/3$ exponent of the velocity–force characteristics around f_c on its behavior close to f_0 : $\Delta X \propto (f - f_0)^{2/3}$.

The dependence of f_c and $f_0(k_S)$ with k_L is presented in Fig. 8. Both f_c and f_0 decrease as k (or $k = k_L$) is increased, nevertheless,

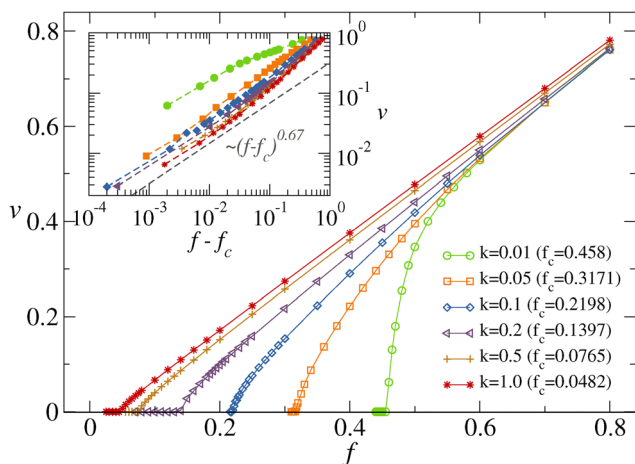


Fig. 6 Depinning model. Velocity–force characteristics (v vs. f) for the 2D elastic interface model of depinning, at different values of the short-range elastic interaction constant k . The inset shows v vs. $f - f_c$, where $f_c = f_c(k)$ depends on k . The dashed line displays a law $v \sim (f - f_c)^{0.67}$. Data corresponds to a system of size $N = 128 \times 128$.

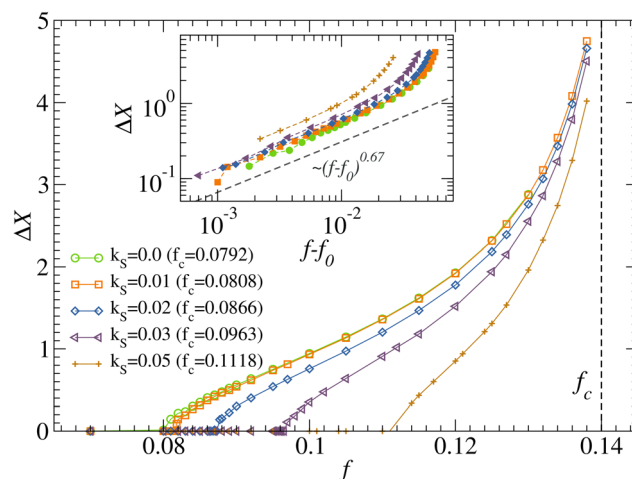


Fig. 7 Depinning model. Interface advance ΔX vs. (sub-critical) applied force f when cycling between a fixed $k_L = 0.2$ and different values of k_S . The inset displays ΔX vs. $f - f_0$. The power-law $\sim (f - f_0)^{2/3}$ is displayed as guide to the eye. Data corresponds to a system of size $N = 128 \times 128$.

f_0 drops faster, specially when the oscillation amplitude ($k_L - k_S$) is large. The difference between f_c and f_0 for a given k_L allows for a window of finite advance ΔX of the interface through the mechanisms of athermal reptation facilitated by oscillations of k . As in the yielding case, for any fixed value of k_S the value of $\eta \equiv (f_c - f_0)/f_c$ decreases as k_L does. Again, the mean field results in Section VII suggest that η is different from zero for any $k_S < k_L$.

VI. Criticality at f_0

The form of the flowcurves above and close to the depinning critical value f_c (σ_c for yielding) is characterized by an exponent β , which contains information about the criticality of the depinning (or yielding) transition:

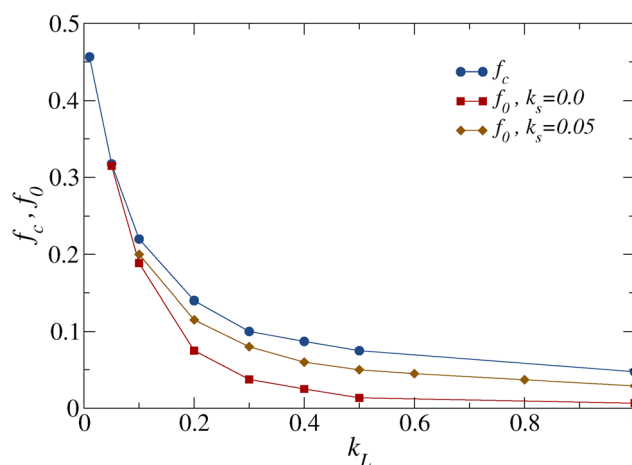


Fig. 8 Depinning model. Critical force f_c (blue circles) and f_0 (red squares for $k_S = 0$, chocolate diamonds for $k_S = 0.05$) vs. k_L . System size used is $N = 128^2$.

$$v \sim (f - f_c)^{\beta_d}; \quad \dot{\gamma} \sim (\sigma - \sigma_c)^{\beta_y}. \quad (7)$$

We have seen that, when analyzing the curves depicted by the sub-critical advance per cycle ΔX (by oscillations in k) close to f_0 , they also look as power-laws. Moreover, the exponents β ($\beta_d \sim 2/3$ for depinning and $\beta_y \sim 3/2$ for yielding) seem to be conserved (within the precision of our numerical data), namely

$$\Delta X \sim (f - f_0)^{\beta_d}; \quad \Delta \gamma \sim (\sigma - \sigma_0)^{\beta_y}. \quad (8)$$

This similarity raises the question about the possibility of having a criticality analogous to the one of the parent transition (depinning/yielding) but at f_0 (σ_0) in the problem of sub-critical advance with oscillations in k . We present now further evidence of criticality around f_0 (σ_0), which favors the hypothesis that the parent transition at f_c (σ_c) is translated somehow to the new (lower) thresholds when oscillations in the environmental conditions step in.

For depinning with constant k it is well known that, in analogy with equilibrium critical phenomena, there is a correlation length ξ diverging at f_c as $\xi \sim |f - f_c|^{-\nu}$ in the thermodynamic limit, which is the hallmark of criticality in the system.^{41,52} One way to assess this correlation length is to evaluate the interface width w as a function of f , which close to f_c is expected to scale as $w \sim \xi^{d+\zeta}$, with ζ the roughness exponent.^{13,43} We may ask if a similar divergence exists in the case of subcritical interface advance under cycling of k , but now around $f = f_0$. Using the standard definition of width

$$w^2 \equiv \overline{x_i^2} - \bar{x}_i^2, \quad (9)$$

we investigate the value of w as a function of f , in finite systems of different sizes and comparing the cases of fixed and cycled values of k .

In the case of a constant k we proceed in the following way. We start at $f = 0$ with a flat interface ($x_i = 0$) and allow the interface to adapt to the pinning forces. Then, f is increased slowly, allowing for the interface to reach a stationary configuration and calculating the value of w at each f . As long as $f < f_c$, the interface reaches a static equilibrium configuration, with w increasing with f . When $f > f_c$ the interface is dynamically evolving with time, and the value of w decreases with respect to its value at f_c .⁵³ The results we obtained are shown in Fig. 9. A sharp maximum of w around f_c is clearly observed, as a sign of criticality. Consistently with what is expected, the maximum of $w(f)$ increases with system size. Moreover, we can study how $w(f)$ behaves around $f = f_c$. For depinning one expects $w \sim \xi^\zeta$ and $\xi \sim |f - f_c|^{-\nu}$, therefore $w \sim |f - f_c|^{-\nu\zeta}$, which in the case of $d = 2$ short-range depinning¹³ ($\zeta = 0.75$, $\nu = 0.8$) results in $w \sim |f - f_c|^{-0.6}$. This behavior is reasonably observed in the data off Fig. 9.

Then, we perform a similar analysis when cycling k between k_L and k_S . The protocol is unchanged with respect to the constant k case, with the important clarification that values of w are now taken stroboscopically in the moments when $k = k_L$.⁵⁴ Values of the width w in the oscillatory regime are shown in Fig. 9 alongside those obtained at fix k . We clearly observe a peak of the interface width at f_0 , that separates the regions of no cyclic advance ($f < f_0$) from that of cyclic interface advance

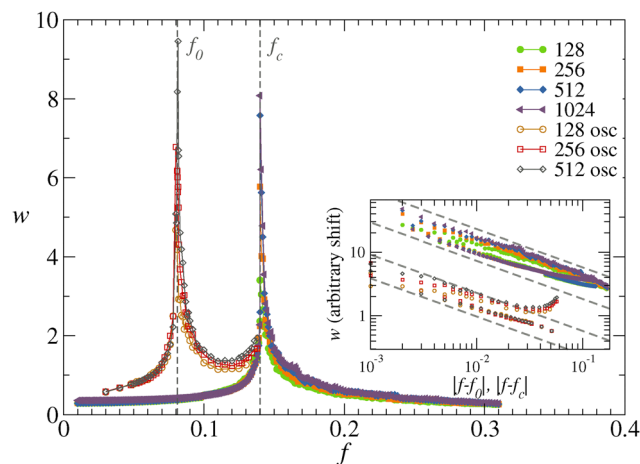


Fig. 9 Depinning model. Interface width w as a function of force for both constant $k = k_L = 0.2$ and cyclic k (between k_L and $k_S = 0$), and different system sizes. Vertical dashed lines mark the location of f_c and f_0 . The inset shows w vs. $|f - f_c|$ or $|f - f_0|$ in log-log scale (both 'from-the-right' and 'from-the-left' branches are shown for each peak, and curves corresponding to the peak at $f = f_c$ are shifted up a factor of ten for a better visualization). The gray dashed lines there correspond to $w \sim |f - f_c|^{0.6}$.

($f > f_0$). The values of w diverge at f_0 in a way compatible with the expression $w \sim |f - f_0|^{-0.6}$. This suggests that we are in the presence of a critical configuration of the interface at f_0 when cycling k , analogous to the critical configuration at f_c under constant k .

Switching now to the case of yielding, let us start by recalling some inherent problems with the definition of the interface width w in such case. As it is well known, the Eshelby kernel possesses soft modes⁵⁵ (*i.e.*, directions in \mathbf{q} space with vanishingly small energy) that are responsible for an unbounded increase of the interface width in time, when the interface is moving. This causes the value of w to be ill defined, since it typically increases in a diffusive way with time. However, this occurs only in the moving phase (*i.e.*, for $\sigma > \sigma_c$ in the constant k case, or $\sigma > \sigma_0$ in the cycling case), whereas the value of w can still be defined below the critical values σ_c or σ_0 . Therefore, for yielding we present results only in those regions of applied stresses. Fig. 10 shows the results obtained for the width w of the elastic manifold in the elastoplastic model simulations (using the same definition as for depinning, eqn (9)). We see a divergence of w close to σ_c for the constant k , and a similar one close to σ_0 for the oscillating k situation of the kind $w \sim (\sigma - \sigma_{c,0})^{0.23}$.⁵⁶ As in the depinning case, this suggests a critical configuration of the interfaces at σ_0 under oscillation of k , similar to that occurring at σ_c under constant k .

The finding of a novel critical point at f_0 (σ_0) in the oscillatory simulations with apparently similar criticality as that f_c (σ_c) is one of the most intriguing outcomes of our investigation. All our results have been presented for a kind of disorder potential that we have called "cuspy" in previous works.^{37,38,47} Essentially, disordered potentials composed by concatenation of parabolic wells. This means that there is an abrupt transition when particles jump out of one well since the

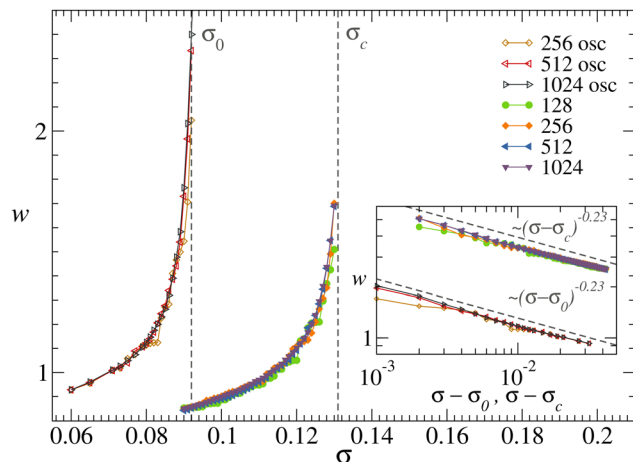


Fig. 10 Yielding model. Yielding strain manifold width w vs. σ for both constant $k = k_L = 3.0$ and cyclic k (between k_L and $k_S = 0.5$), and different system sizes. Vertical dashed lines mark the location of σ_c and σ_0 . The inset shows w vs. $\sigma - \sigma_c$ or $\sigma - \sigma_0$ in log–log scale and the gray dashed lines there correspond to $w \sim (\sigma - \sigma_c)^{0.23}$ (curves corresponding to the peak at $\sigma = \sigma_c$ are shifted up a factor of three for a better visualization).

potential has a discontinuous derivative at the cusp. We have argued^{37,47} that in the case in which these potentials are smooth, the criticality at f_c – in particular the value of the β exponent of the velocity–force characteristics – changes. Therefore, a natural step to verify if the coincidence of the universality at f_0 and f_c is a robust feature, would be to study a model using cuspy and smooth potentials and see if the exponents change consistently in both f_c and f_0 . A detailed study of cuspy vs. smooth potentials in spatial yielding and depinning systems in the context of the oscillatory creep is left for future works, but here as a proof of concept, we test the hypothesis in the simplest case of mean field depinning, fully connected interactions. The results are presented in Appendix B and interestingly they indicate that when cycling k , we find the same critical exponents around f_0 as those at the classical velocity–force characteristics at f_c ($\beta = 1$ for cuspy potentials and $\beta = 3/2$ for smooth potentials). This, in fact, strengthens the idea that cyclic variations of internal parameters (as the elastic constant k) can effectively cause a ‘shift’ of the flow threshold, depleting the critical point, which brings with it the criticality, that is preserved. And, at the same time, it shows the robustness of our results respect to the choice made to take stochasticity into account in the models.

VII. The reptation mechanism in a mean-field approach

The results in the previous sections concerning spatially distributed depinning and yielding models are the closest to geophysical application and can serve as a starting point for more realistic studies. Nevertheless, we think it is conceptually valuable to complement those results with a mean-field approximation. This will give insight into the mechanism of sub-critical deformation, and will also allow us to analytically

verify some of the claims that we made in the presentation of results for spatially extended models.

Let us consider a system of N particles characterized by their coordinates x_i ($i = 1, \dots, N$) interacting elastically. The mean field nature of the model is contained in the form of the elastic interaction, that produces an elastic force on each particle given by

$$f_i^e = k(X - x_i) \quad (10)$$

where $X = N^{-1} \sum_i x_i$ is the average position of the interface. Furthermore, in the present section we take the potential $V_i(x_i)$ of interaction with the substrate to be a collection of narrow wells randomly distributed along the x_i coordinate with a mean separation a . This can be thought to correspond to a limit in which the parabolic wells used previously become very narrow. The wells are characterized by the force f_p that must be applied to a particle trapped in the well to escape from it. For simplicity, we take the value of f_p to be the same for all wells, stochasticity is guaranteed by the random position of the wells. In addition, an external force f is assumed to be applied to the particles.

In the narrow well approximation the dynamical evolution equation (of the kind of eqn (4)) is replaced by a discrete rule, defined in the following way. If a particle is inside a potential well, it remains there as long as the absolute value of the force on the particle $F_i \equiv f + f_i^e$ is lower than the pinning force f_p . If $|F_i| > f_p$, in a single time step the particle jumps (towards the right or the left according to the sign of F_i) to the equilibrium point where $F_i = 0$, namely $\tilde{x}_i = f/k + X$, or to a new potential well if it happens to reach one in between x_i and \tilde{x}_i .

The critical force f_c in this model is the maximum value of f for which a stationary (non-moving) situation can be found, namely a configuration in which all sites have either $|F_i| < f_p$ and are within pinning centers, or have $F_i = 0$. The value of f_c can be obtained analytically (see Appendix C). Introducing the rescaled variable

$$z = \frac{ka}{f_p} \quad (11)$$

one obtains that f_c is given by

$$f_c = f_p(1 - z + ze^{-1/z}). \quad (12)$$

Now, we introduce in the model the variation in time of the spring constant k , considering a cyclic variation between a large value k_L , and a small value k_S , and take this variation to occur quasi-statically, this is, not introducing effects associated to the velocity of variation. The process can be analyzed qualitatively as follows (Fig. 11). We suppose that the system is under an applied force f that is lower than f_c for all values of k in the range $k_S - k_L$ (in practice, this means that f is lower than the f_c corresponding to k_L). In Fig. 11(a) we sketch a configuration of the system at a large value k_L of k . This is a stable configuration, with some particles at pinning centers, and some others outside them. In Fig. 11(b) we depict the configuration of the system when k has been reduced to a value k_S that for a simpler analysis has been taken to be zero. Sites that were pinned in (a)

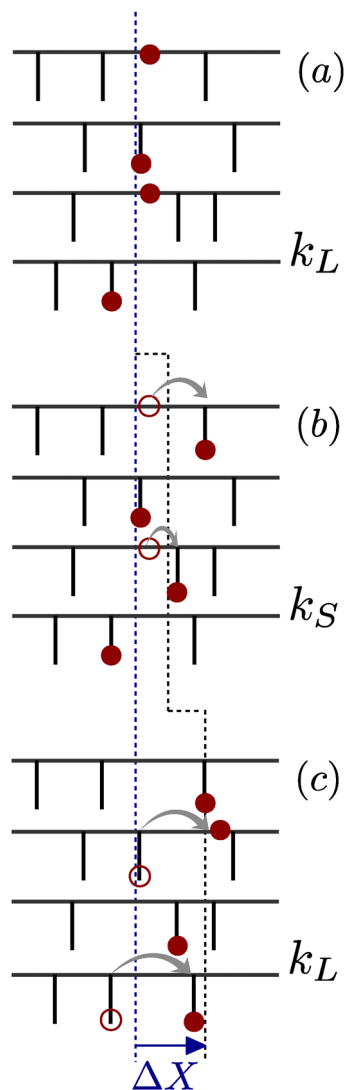


Fig. 11 Qualitative evolution of the configuration of the system when k passes from a high value k_L (a) to a small one k_S (b) and increases again to k_L (c). A constant stress f (pointing to the right) is present in all cases. Although the parameters of the system in (a) and (c) are identical, the system configuration is not, the mean position moved to the right by ΔX .

remain pinned at the same well, but those that were unpinned were dragged to the right by f , and each one reaches the first available well, where it gets pinned. In Fig. 11(c) the value of k is increased again to k_L and some particles (those located in the left-most wells) jump out of their pinning centers, as the total force on them is larger than f_p . The system accommodates in a new equilibrium configuration (c) that is not coincident with the one in (a), although the parameters in (c) are the same as those in (a). Therefore, there is a finite shift in the mean position of the interface $\Delta X \equiv X_c - X_a$. If the cycling of k between k_L and k_S is repeated, a shift ΔX is expected to occur on each cycle. The value of ΔX will be larger when f is close to f_c and will be smaller as f is decreased away from f_c . This is expected, since f is the driving force for the increase of X on each cycle of variation of k .

By the treatment presented in Appendix C we have been able to derive analytically the form of ΔX as a function of f ($f < f_c$) in the case in which $k_S = 0$. This is shown in Fig. 12 with the continuous red line. This analytical result is very important as it shows that there is in fact a minimum value f_0 that has to be exceeded to have a finite value of ΔX . The analytic form of f_0 (eqn (C5)), together with eqn (12) for f_c are plotted in Fig. 13. Although the two curves become very close as k_L approaches zero, they remain different for any $k_L \neq 0$. We believe this also occurs in the depinning and yielding cases (Fig. 5 and 8); notice that curves there show data obtained at fixed values of k_S and not relative to k_L , therefore the behavior is not as evident as in Fig. 13.

We complement the analytical results with numerical simulations to obtain the value of ΔX as a function of the values k_L and k_S , at different values of the applied force f . A system with $N = 10^5$ sites is simulated following the rules explained at the beginning of the section. First, a value of $k = k_L$ is chosen and some $f > f_c$ is applied during a number of steps to obtain a steady state. Then we reduce progressively f repeating the procedure and measuring in the steady states to obtain the flow curve. When f becomes lower than f_c , X sets to a constant value. Starting from this initial configuration we slowly cycle k between k_L and k_S and obtain the average advance of the interface ΔX per cycle.

When $f > f_c$, the deformation of the system increases at a finite rate with time, defining the flow curve \dot{X} vs. f . This is plotted in the right part of Fig. 12 for different values of the parameter k . As in the spatially extended models for depinning and yielding of previous sections, we see how lower values of k displace the curves to the right: softer elastic interaction gives possibility to the system to accommodate better to the pinning potential and the necessary stress f_c to produce a finite deformation velocity increases. The results for ΔX are displayed in the left part of Fig. 12, where ΔX is shown as a function of f ,

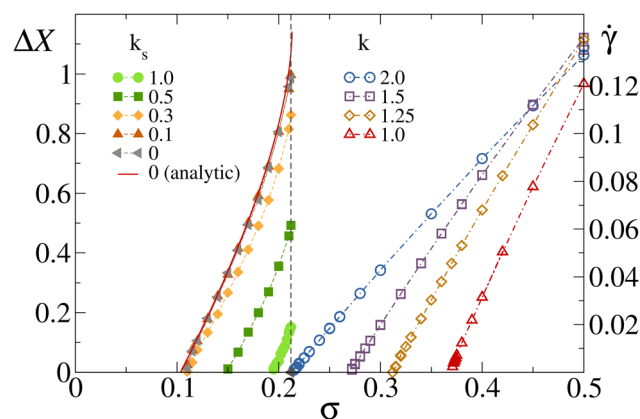


Fig. 12 Fully-connected depinning model. (right) Numerical flow curves of the system at different values of k . (left) Interface advance ΔX per cycle, as a function of applied force f when the interface stiffness is cycled between $k_L = 2$, and values of k_S as indicated. Points are the results of numerical simulations. The continuous red line is the analytical result for $k_S = 0$ (see Appendix C).

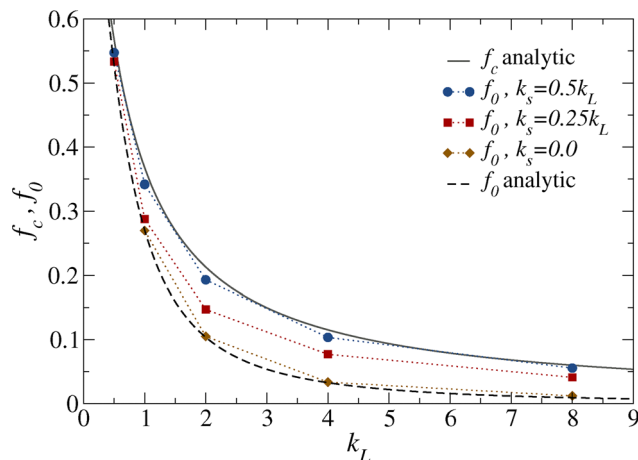


Fig. 13 Fully-connected depinning model. Critical force f_c as a function of k_L (gray line, analytical result), reptation limit f_0 as a function of k_L (black-dashed line, analytical result), and numerical results for f_0 when cycling the system between k_L and k_S as indicated in the labels.

when k is cycled between a value $k_L = 2$, and different values of k_S . For $k_S = 0$ the numerical results nicely reproduce the analytical ones. When $k_S > 0$ the range $f_0 - f_c$ in which the effect is observed is reduced.

In Fig. 13 we also show results of numerical simulations for f_0 and f_c . We see that numerical and analytical values of f_c as a function of $k = k_L$ agree very well. The same occurs for f_0 when $k_S = 0$. The region between f_0 and f_c is the range in which there is a non-zero advance ΔX for each cycle of variation of k .

VIII. Discussion and connection with related phenomena

Let us now emphasize similarities and differences between the mechanism of sub-critical flow or reptation presented here and other cases that have been considered previously in the literature. As stated in the introduction, external mechanical noise has been studied as a possible driver of sub-critical flow in soft-glassy materials. In many cases, external noise is assumed to act randomly in time and/or space, making its effect similar to that of thermal noise, apart from differences in relative intensity.^{23,24,57} In other cases, the external perturbation acts rather homogeneously across the system, as for instance in the case of cyclic loading,^{58,59} or when a “tapping” noise is applied.¹⁵ In addition, “noise” has been applied on top of an average external stress as a stochastic contribution,⁶⁰ or simply as a serrated contribution to the stress.⁶¹ In this last case a viscous response directly related to small stress modulations and consequently ‘flow’ below the yield stress is found, in a scenario described as a ‘secular drift’ or ratcheting process at long times.

The key distinction between previous scenarios and our results is that we consider a perturbation (the variation in the elastic stiffness k of the system) that acts in a quasi-static limit, meaning it has no effects associated with its rate of change. In addition, this perturbation is homogeneously applied to the

whole system, and it can be considered to be rooted in variation of environmental conditions. We have described our mechanism as a “reptation” process, which is an image particularly adapted to the two-particle model of Section II, as well as for the model system described by Moseley.³³ Yet, the full models of depinning and yielding that we considered can be qualitatively described by the same basic mechanism.

It is worth commenting on the literature on thermally cycled granular systems.^{26–32} Some experimental setups incorporating thermal cycling are related to pile compaction,^{26,32} while others analyze ratcheting displacement by including a lateral forcing on a body resting on the granular system,²⁸ and could bare more similarity with the downhill soil creep. In all these cases, the periodically oscillated environmental variable is the external temperature and its variations have proved to induce macroscopic volumetric expansion and contraction cycles which can induce irreversible deformations in granular systems such as sand, silts and clays.³⁰ While the microscopic origins of the macroscopic response remains somehow elusive,³¹ X-ray microtomography has revealed already that interactions happening at the particle level are key: the material’s thermally induced deformations (*e.g.* compaction) are strongly dependent on particles shape,^{31,32} as well as on relative density and the prescribed temperature amplitude itself.^{30,32} Conceptually, it is not difficult to accept that consecutive periods of expansion and contraction of the granular material would produce, at least at a mesoscopic length scale, a modulation in the region-to-region elasticity propagator, which is what the models incorporate in a simplified approach to the real materials.

There is a remarkable similarity between the sub-critical flow mechanism described here and the phenomenon of cyclic fatigue in material science.⁶² In fact, the cyclic fatigue phenomenon typically refers to the systematic increase in the length of micro-cracks by a fixed amount⁶³ at every cycle of increase and decrease of the stress applied to a sample. There is a strong analogy between this process and the finding of a constant increase ΔX under increase and decrease of spring constants in our case. Also, the finding of a lower force/stress value (f_0 or σ_0) below which oscillation of the spring constant does not produce any average deformation is qualitatively similar to the concept of “fatigue limit” (also known as intrinsic strength for polymeric materials, see ref. 64 and 65). Namely, a stress amplitude below which cracks in a material do not display any advance. Yet one difference is that cracks do not form in our set up, since the detaching of particles from their potential wells is followed by the re-attaching to a new well at a different position. Another difference is that in the fatigue scenario it is the stress amplitude itself that gets temporal variations, while there are no changes in intrinsic parameters of the system. In contrast to hard and fragile materials, soft glassy materials – in particular gels⁶⁶ – might be a good benchmark to compare the characteristics of cyclic fatigue with those of the sub-critical flow we describe in this work, as such systems (within some experimental conditions) can also flow continuously without irreversible failure, and therefore reach flowing steady-states. Fiber bundle models⁶⁷ are a particularly useful benchmark to

study the possible effect of oscillatory variation of parameters leading to fatigue failure. We plan to explore further this analogy, also considering cases where the perturbation takes the form of an externally oscillating stress, either aligned with or in a different direction from the average stress. This will bring our case much more similar to the fatigue scenario. In addition, results on shear-oscillated granular systems⁵⁹ showing that particle roughness on a given length-scale could effectively affect the energy landscape and facilitate flow below the expected critical amplitude could constitute interesting analogous cases of critical threshold depletion. On the theoretical side, it would be interesting to analyze the mechanically stable configurations both below and above f_0 during the oscillatory protocol in the context of the Edwards thermodynamics.⁶⁸

IX. Summary and conclusions

In this work, we investigated a mechanism for athermal, sub-critical material flow driven by periodic variations in a parameter that affects internal structural forces in an externally driven system. We illustrated this mechanism using a minimal model: two particles connected by a spring of variable stiffness k , which undergoes reptation down an inclined plane with a finite displacement ΔX per cycle of periodic variation in k . We then extended this oscillatory mechanism to spatially distributed models of depinning and yielding transitions.

We demonstrated that when the external driving force f is below the critical threshold f_c required for a steady deformation with time at a finite rate ($dX/dt > 0$), there is a regime in which the system exhibits synchronized evolution with the periodic variation of k , which represents the global elastic rigidity. The deformation per cycle, ΔX , decreases as f is reduced and vanishes at a well-defined threshold, f_0 . These results were obtained numerically and also analytically in a mean field version of the problem.

The discovery of a sharp f_0 value that separates a long-lasting evolving regime from a non-evolving one is particularly remarkable. This behavior is fundamentally different from thermal creep, where thermal activation always induce a finite creep rate, even at arbitrarily low f (although vanishingly small as f is reduced). Furthermore, the similarity between the behavior of ΔX near f_0 under variation of k and that of v near f_c for fixed k suggests that the system may exhibit criticality at f_0 , analogous to its critical behavior at f_c . Our analysis of the elastic roughness near f_0 revealed a divergence in the interface width w , a key indicator of criticality. Current results suggests that the critical exponents at f_0 may be the same as those at f_c , though further detailed numerical analysis is required to confirm this.

Our findings have potential implications for interpreting geophysical processes at the Earth's surface. While the persistent downhill creep of natural soils remains a subject of study, laboratory experiments suggest that environmental disturbances play a crucial role. In particular, Deshpande and co-workers¹⁵ assign to daily temperature fluctuations the ability to 'rejuvenate' the sandpiles through thermomechanical stresses

and sustain an approximately constant creep rate through repeated heating and cooling cycles. This phenomenon is not yet fully understood, but we believe to be widespread, extending beyond specific materials and experimental setups.

The mechanism we propose involves periodic variations in internal parameters that modulate inter-particle or inter-regional forces, which facilitates the system reptation or flow. The timescales associated with this sub-critical displacement are tightly coupled to the period of parameter oscillation, suggesting that similar mechanisms could operate in natural environments, linked to daily, seasonal, or even geological-scale cyclic variations. Our modeling approach, where an interaction spring constant changes in an adiabatic manner, provides a simplified but well-founded framework for capturing sub-critical flow driven by environmental conditions such as temperature and humidity. Our hypothesis, supported indirectly by observations in thermally cycled granular systems, posits that periodic environmental changes induce periodic oscillations in the systems effective internal parameters. We demonstrated that this effect is relevant in models of driven elastic interfaces in disordered media and in models of amorphous solids under deformation, revealing a regime of externally driven sub-critical flow that remains entirely athermal. The connection between environmental variability and internal elasticity is key and warrants further systematic study; *e.g.*, the existence of a finite threshold σ_0 below which the creep by variations of environmental changes vanishes remains something to be tested in the lab. Furthermore, our generic results suggest looking for particular models to describe specific types of oscillatory perturbations, such as: particles with quasi-static size oscillations (*e.g.*, due to daily or seasonal thermal expansion) as in ref. 19, clays with adhesion properties modulated by humidity changes, and systems with oscillating confinement geometries (*e.g.*, periodically moving lateral boundaries). While the specifics may vary, we expect the underlying physical mechanism to remain qualitatively the same.

Conflicts of interest

There are no conflicts to declare.

Data availability

The code used for the simulations can be found at <https://bitbucket.org/ezeferro/athermalcreep> and raw data supporting this article have been included as part of the ESI.†

Appendices

A. Simulation details and varying k protocol

The models used for both depinning and yielding transitions have been presented in Section III. In this Appendix we provide some details regarding the simulations and parameters used, as well as an analysis of the frequency dependence of the subcritical creep in the oscillatory k protocol.

One specification to be made is that when working with long-range interactions, *i.e.*, in the elastoplastic model for the yielding transition, we make use of a pseudospectral method. This is, the Eshelby kernel is defined in Fourier space as

$$G_q^Y = k \frac{(q_x^2 - q_y^2)^2}{(q_x^2 + q_y^2)^2} \quad (\text{A1})$$

and from here the precise form in real space is obtained (see eqn (6)). Then, at each step of the dynamics, the strain field appearing in eqn (5) is converted to Fourier space and convoluted with the kernel. The result is anti-transformed to get back the elastic interactions in real space.

For the disorder potential energy $V(x)$ appearing both in eqn (4) and (5) we have adopted a function which alternates between parabolic wells and flat regions, as schematically depicted in Fig. 14. All parabolas are taken to be identical, defined by a unitary curvature and unitary width between the starting and ending points of the wells. The inter-wells flat regions, instead, are of different lengths, taken randomly from an exponential distribution, uncorrelated from site to site. This is the element that introduces randomness in the model. We have also tested other types of disorder potentials, as for example the direct concatenation of parabolic wells of different sizes used in previous works.^{11,47} The observed physics does not change qualitatively, but depending on the parameters the sub-critical reptation region can be very narrow and visible only very close to f_c . The intercalation of wells and flat regions somehow helps the elastic manifold systems to enhance the oscillatory creep effect. As a matter of fact, notice that the limit in which the parabolic wells become very narrow ‘traps’ corresponds to the case in which we can build the equivalence between the elastic manifold depinning-like models and the classic elastoplastic models of amorphous solids; these typically use a binary ‘state’ (elastic/plastic) variable for the model building blocks along with the local stress.⁶ Therefore our $V(x)$ choice lays in between the ones typically used for depinning and for yielding and serves well to show the sub-critical reptation effect in both cases.

For a given fixed value of $k = k_L$ in eqn (4)–(6) and $f > f_c$ one can reach a stationary state after a transient by running a simulation for a moderate time, depending on the initial configuration. If the starting condition corresponds to a steady state configuration obtained for a slightly larger force, the new steady state is reached very fast, typically a few hundreds time steps. In fact, that is what we do to obtain the flowcurves of

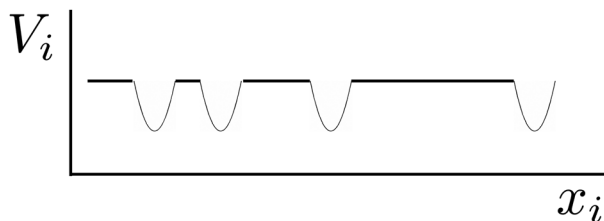


Fig. 14 Schematic representation of the typical disorder potential we use. All parabolic wells are identical. Inter-wells segment lengths are taken randomly from an exponential distribution.

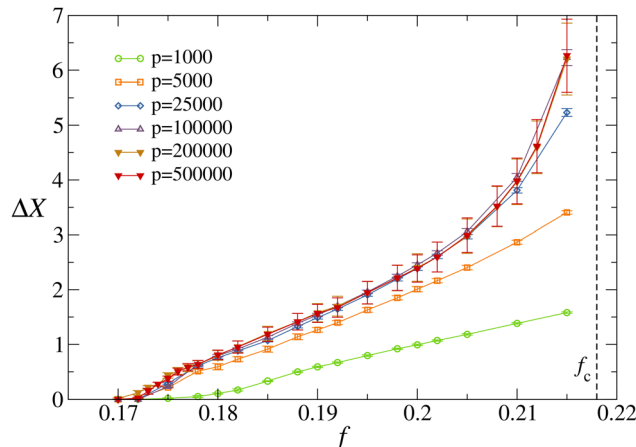


Fig. 15 2D short-ranged depinning model. Dependency of the estimated value of ΔX on the period number p . System size is $N = 512 \times 512$, $k_L = 0.1$, $k_S = 0$.

Fig. 3 and 6: we start at a large force, reach a steady state there and then slightly decrease the force and run stabilization periods at each step to take measurements in the steady states.

On the contrary, reaching a steady state in the oscillatory protocol at $f < f_c$ is not that computationally cheap. First, we have noticed that there is a strong dependency of the obtained values of ΔX (eventually, even of f_0) with the frequency (equiv. period) of oscillation. Fig. 15 shows the frequency dependence of ΔX in the case of the depinning model. If we want to work in an adiabatic limit, the step of change in k should be small enough to have results that are independent of it. Trying to reach such a quasistatic limit, we have chosen the transition between k_S and k_L to be very slow. We have found both for depinning and yielding that a period of 20 000 steps was enough to guarantee frequency-independence in our results within error estimations of ΔX for most forces, and therefore used that value along the study. Nevertheless, for different system sizes, and in particular very close to f_c , this quantity should be adjusted to reach a frequency-independent steady state value. Secondly, once the period is defined, one needs to run a large number of cycles for ΔX and w to actually stabilize in mean value. Typically we use a transient of 500 periods that we discard to reach the steady state and then yet another 500 periods to take measurements and averages.

B. Other disordered potentials and exponents dependency

In order to check if the coincidence of the universality at f_0 and f_c is a robust feature, we study a model using two different types of disordered potentials, which give different values of the flow exponent β in fully connected systems, namely ‘cuspy’ potentials ($\beta = 1$) and ‘smooth’ potentials ($\beta = 3/2$).

In particular we work in this section with disordered potentials of the form:

$$\begin{aligned} V_i(x) &= A_i(x + \phi_i - \lfloor x + \phi_i \rfloor + 1/2)^2 \quad \text{for cuspy} \\ V_i(x) &= A_i \sin(x + 2\pi\phi_i) \quad \text{for smooth} \end{aligned} \quad (\text{B1})$$

where the symbol $[\dots]$ stands for the integer part of the argument, therefore producing a concatenation of parabolic pieces for the cuspy case. The amplitudes A_i and the phases ϕ_i are site-dependent quenched random variables, in the range $[0:1]$.

The system is fully-connected, meaning that every site interacts with each other with the same intensity, resulting in a mean-field interaction where the elastic force on each site is computed respect to the mean position $X \equiv N^{-1} \sum_i x_i$. This yields the equation of motion

$$\frac{\partial x_i}{\partial t} = -\frac{dV_i}{dx_i} + k(X - x_i) + f. \quad (\text{B2})$$

This fully-connected mean field model can also be considered as an instance of the Prandtl–Tomlinson model of friction. For this model, the values of β using cuspy or smooth potentials are known to be $\beta = 1$, and $\beta = 3/2$, respectively.⁶⁹ In this simple case of mean-field interactions, the interface does not have a diverging width at the transition, therefore the comparison of criticality at f_c and f_0 will be limited to compare the values of β .

Fig. 16 and 17 present results of simulations of model (B2) for cuspy and smooth potentials (B1), respectively. As expected, reaching $f = f_c$ from above one obtains a velocity–force characteristics that behaves as $v \sim (f - f_c)^\beta$ with $\beta = 1$ for the cuspy potential and $\beta = 3/2$ for the smooth potential. What is interesting is that in the oscillatory k protocol one can clearly reproduce these same values around the corresponding f_0 in each case. These additional results, constructed with totally different disordered potentials than in the maintext, provide additional support to our main messages: (i) it is possible to obtain a finite displacement below the critical threshold f_c by cycling the strength k of the elastic interactions, (ii) this displacement vanishes at a new ‘critical’ point f_0 but preserving the critical exponents of f_c , whatever they are according to the kind of interactions, dimension and disorder type.

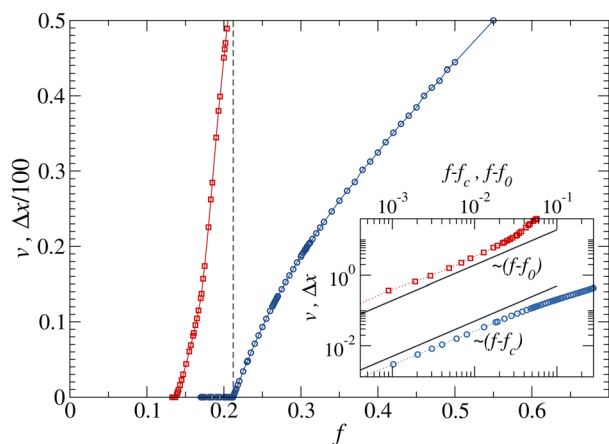


Fig. 16 Velocity–force characteristics for the fully-connected system, with $k = k_L = 0.1$ and $k_S = 0$ and a parabolic disordered potential. The inset shows v vs. $f - f_c$ ($f_c = 0.212$) and ΔX (arbitrarily rescaled) vs. $f - f_0$ ($f_0 = 0.138$). The full lines display the laws $v \sim (f - f_{c,0})$. Data corresponds to a system of size $N = 512 \times 512$.

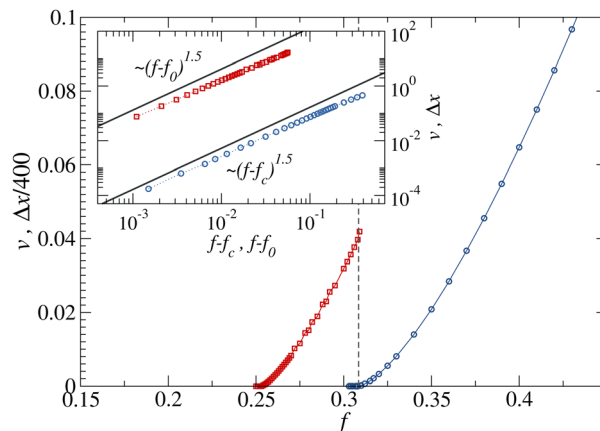


Fig. 17 Velocity–force characteristics for the fully-connected system, with $k = k_L = 0.1$ and $k_S = 0$ and a sinusoidal disordered potential. The inset shows v vs. $f - f_c$ ($f_c = 0.309$) and ΔX (arbitrarily rescaled) vs. $f - f_0$ ($f_0 = 0.253$). The full lines line displays laws $v \sim (f - f_{c,0})^{1.5}$. Data corresponds to a system of size $N = 512 \times 512$.

C. Analytical results in the mean field model

Many details of the mean field model can be worked out analytically. We describe here the kind of treatment that is necessary for these calculations, and present a few results. In particular, we show the existence of a range $f_0 - f_c$ in which there is a cyclic advance of the system upon oscillation of the value of k , and calculate the value of ΔX in this range of applied forces.

As described before, the system consists of N particles that move in a one-dimensional axis x under the action of a potential consisting of a collection of very narrow wells, randomly distributed along x (with a mean separation a , this implies an exponential distribution of inter-well distances). Potential wells have a maximum pinning force that they are able to withstand, that we call f_p , and is the same for all the wells. A particle in a stationary situation can be located within a well (as long as the force acting on it is lower than f_p) or in the region between two wells. In this last case, the position of the particle is determined by the condition that the total force acting on it must be zero.

In the present mean field representation the force acting on particle i is

$$f_i = k(X - x_i) + f \quad (\text{C1})$$

with $X = N^{-1} \sum_i x_i$ being the average coordinate position of the system. Note that this force is linear in x_i (see Fig. 18). Given any initial condition, upon setting a global $f > 0$, all particles advance to the right until an equilibrium is reached. This occurs when every particle has either reached a well from which it cannot escape and $f_i < f_p$, or, on its path to the next well, has reached the position with $f_i = 0$, and stays there. The position $x \equiv x_\delta$ where this happens has to adjust to the condition $f + k(X - x_\delta) = 0$. Therefore, particles that are outside wells are all located at this same position. Introducing the function $P(x)$ that gives the probability distribution of finding a particle at coordinate position x , a bit of analysis leads to the

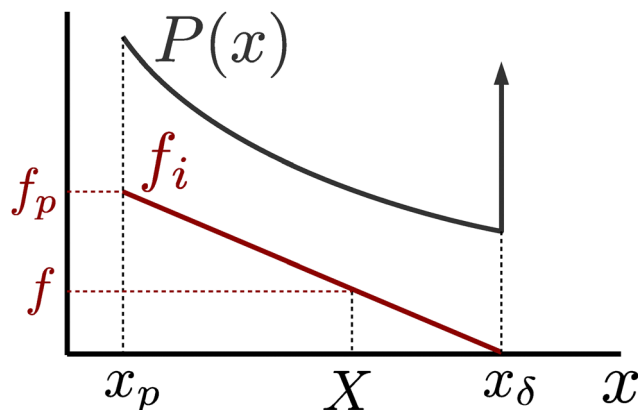


Fig. 18 Schematic representation of the probability distribution function $P(x)$ for a system at the critical force f_c . Note that $P(x)$ consists of the continuous black line plus the delta peak at the right. The red line shows the x -dependent force on the particles f_i , which is equal to f_p at the left-most point of the distribution, zero at the delta peak, and the externally applied force f at X .

conclusion that the $P(x)$ consist of an exponential piece (originated in the exponential distribution of the inter-well distances), plus the delta peak populated by the particles that are outside wells (see Fig. 18). The exponential part of $P(x)$ starts at the point defined as $x \equiv x_p$, where the force equals f_p , and extends to the point $x = X + f/k$ where the force is zero and where the delta peak locates. In other words, at fixed k and f , particles outside wells are always the most advanced ones.

Let us consider the situation of a system driven just above the critical force: $f = f_c$. When $f \lesssim f_c$, the most retarded particles (namely most to the left along the x axis) are trapped in a well and supporting the largest elastic force. In the continuous evolution of the system, when f just overcomes f_c and a finite global velocity is set, those particles are the first to jump out of their wells, given that all wells have the same pinning force f_p . When they jump out, they reach the next well to the right, or stay at the point where $f_i = 0$ if this happens before (to the left of) the next well. Note that in the present case eqn (C1) implies $f_p - f_c = (X - x_p)k$. From its very definition, we also have $X = \int x P(x) dx$. Introducing the form of $P(x)$ and after a bit of manipulation and combination with the previous expression we obtain the value of the critical force as

$$f_c = f_p(1 - z + ze^{1/z}) \quad (\text{C2})$$

with $z \equiv kalf_p$.

Let us now analyze the case in which a value $f < f_c$ is applied and the value of k is cycled quasi-statically between a large (k_L) and a small value (k_S). For simplicity we describe the situation when k_S is zero (Fig. 19). Provided an initial condition in equilibrium at a non-zero applied force $f < f_c$ pointing to the right and $k = k_L$, we start from a $P(x)$ distribution similar to that of Fig. 18. Reducing the value of k to zero does not affect the position of particles that are located inside wells, but those that were at the delta peak of $P(x)$ now drift towards the right until they find a new potential well. In the end, for $k = 0$ the $P(x)$ distribution becomes a pure exponential $P(x) \sim e^{-x}$ starting at

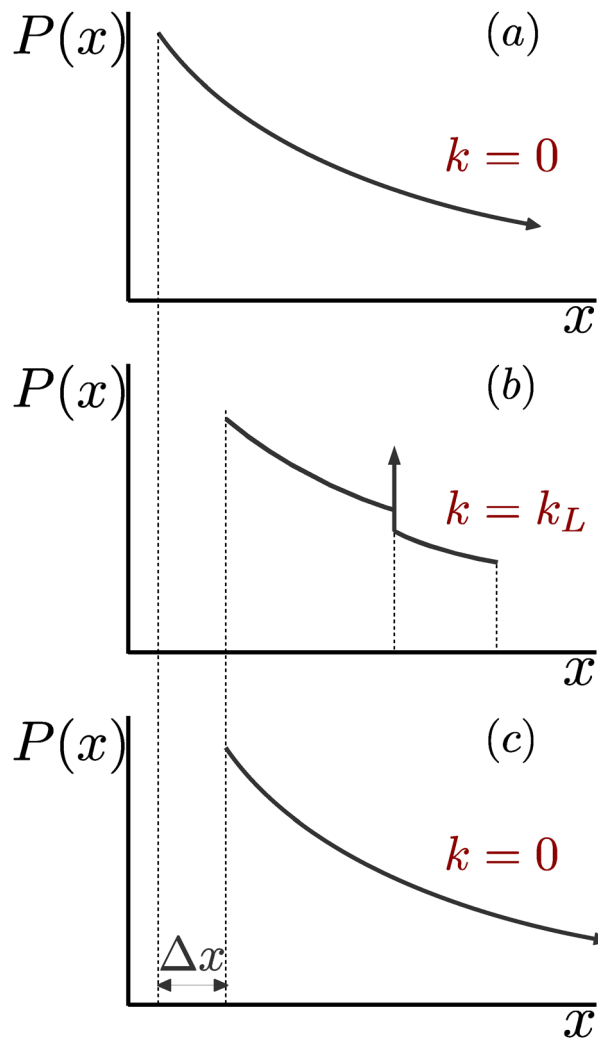


Fig. 19 Schematic evolution of $P(x)$ for an applied force f ($f_0 < f < f_c$). (a) Distribution at $k = k_S \equiv 0$. This is a purely exponential distribution. (b) Distribution at $k = k_L$. Some of the right-most particles in (a) have jumped back to the position where $f_i = 0$. Others from the left-most part have moved to the right. (c) Distribution when k is set back to $k_S \equiv 0$. The distribution is similar to that in (a), but displaced to the right a distance Δx .

some given point x_0 . This is indicated schematically in Fig. 19(a). Note also that from the history of the dynamical evolution, given a particle located at a well at x_i , we can be sure there is no other well for that particle in the interval (x_0, x_i) . Now, when the value of k is increased again ($k \rightarrow k_L$), the elastic force start to act on the particles. All those on the right of the mean value X will feel a force pushing them to the left, and for those with the largest values of x such force would overcome $-f_p$ and they will jump out of their wells but now towards the left. Because of the previous comment, those particles do not reach a new well but regain a position in which $f_i = 0$ for such $k = k_L$, creating a delta peak at a position that now is intermediate in $P(x)$ (those particles feeling a force $0 > f > -f_p$ persist in their wells and have $x > x_\delta$). Along this process, it may happen (and it happens eventually, *i.e.*, when $f > f_0$) that some of the left-most particles receive a positive force larger

that f_p , and they jump to the right (dragged by a mean value X that has moved forward in the previous step). The final distribution at $k = k_L$ is qualitatively seen in Fig. 19(b). Finally, when k is turned to zero again, the process is repeated but with some particles already advanced respect to the previous cycle. We obtain the result in Fig. 19(c), namely a distribution similar to the one in Fig. 19(a), but displaced to the right in an amount ΔX .

Based in the qualitative evolution just mentioned, it is possible to calculate the value of ΔX given the value of k_L . The calculation is elemental, but a bit cumbersome. The outcome is the following. First, one calculates \tilde{z} from

$$f/f_p = 1 - \tilde{z} + (1 + \tilde{z})e^{-2/\tilde{z}}. \quad (C3)$$

Then, ΔX is calculated from

$$f/f_p = 1 - z + ze^{-1/z}(1 - e^{-\Delta X}) + (2z/\tilde{z} - 1 + z - z\Delta X)e^{-2/\tilde{z}}. \quad (C4)$$

The obtained $\Delta X(f)$ curve is plotted in the left panel of Fig. 12. In particular, setting ΔX to zero provides the minimum value f_0 necessary to observe the advance of the system upon oscillation of k , which is

$$f_0 = f_p(1 - z + (1 + \tilde{z})e^{-2/\tilde{z}}). \quad (C5)$$

This dependence was shown in Fig. 13.

Acknowledgements

We acknowledge support from PIP 2021–2023 CONICET Project No. 757 and the CNRS IRP Project “Statistical Physics of Materials”. EEF acknowledges support from the Maria Zambrano program of the Spanish Ministry of Universities through the University of Barcelona, and MCIN/AEI support through PID2019-106290GB-C22 and PID2022-137505NB-C22. We acknowledge computational resources provided by the HPC cluster of the Physics Department at Centro Atómico Bariloche.

References

- 1 K. E. Daniels and D. J. Jerolmack, Viewing earth's surface as a soft-matter landscape, *Nat. Rev. Phys.*, 2019, **1**, 700.
- 2 A. Voigtländer, M. Houssais, K. A. Bacik, I. C. Bourg, J. C. Burton, K. E. Daniels, S. S. Datta, E. Del Gado, N. S. Deshpande, O. Devauchelle, B. Ferdowsi, R. Glade, L. Goehring, I. J. Hewitt, D. Jerolmack, R. Juanes, A. Kudrolli, C.-Y. Lai, W. Li, C. Masteller, K. Nissanka, A. M. Rubin, H. A. Stone, J. Suckale, N. M. Vriend, J. S. Wettlaufer and J. Q. Yang, Soft matter physics of the ground beneath our feet, *Soft Matter*, 2024, **20**, 5859.
- 3 A. Young, Soil movement by denudational processes on slopes, *Nature*, 1960, **188**, 120.
- 4 M. Kirkby, Hillslope process-response models based on the continuity equation, *Inst. Br. Geogr. Spec. Publ.*, 1971, **3**, 5.
- 5 D. Bonn, M. M. Denn, L. Berthier, T. Divoux and S. Manneville, Yield stress materials in soft condensed matter, *Rev. Mod. Phys.*, 2017, **89**, 035005.
- 6 A. Nicolas, E. E. Ferrero, K. Martens and J.-L. Barrat, Deformation and flow of amorphous solids: Insights from elastoplastic models, *Rev. Mod. Phys.*, 2018, **90**, 045006.
- 7 M. Popović, T. W. J. de Geus, W. Ji, A. Rosso and M. Wyart, Scaling description of creep flow in amorphous solids, *Phys. Rev. Lett.*, 2022, **129**, 208001.
- 8 C. Liu, E. E. Ferrero, K. Martens and J.-L. Barrat, Creep dynamics of athermal amorphous materials: a mesoscopic approach, *Soft Matter*, 2018, **14**, 8306.
- 9 J. Weiss and D. Amitrano, Logarithmic versus andrade's transient creep: Role of elastic stress redistribution, *Phys. Rev. Mater.*, 2023, **7**, 033601.
- 10 M. Popović, T. W. J. de Geus, W. Ji and M. Wyart, Thermally activated flow in models of amorphous solids, *Phys. Rev. E*, 2021, **104**, 025010.
- 11 E. E. Ferrero, A. B. Kolton and E. A. Jagla, Yielding of amorphous solids at finite temperatures, *Phys. Rev. Mater.*, 2021, **5**, 115602.
- 12 P. Chauve, T. Giamarchi and P. Le Doussal, Creep and depinning in disordered media, *Phys. Rev. B: Condens. Matter Mater. Phys.*, 2000, **62**, 6241.
- 13 E. E. Ferrero, L. Foini, T. Giamarchi, A. B. Kolton and A. Rosso, Creep motion of elastic interfaces driven in a disordered landscape, *Annu. Rev. Condens. Matter Phys.*, 2021, **12**, 111.
- 14 E. E. Ferrero, L. Foini, T. Giamarchi, A. B. Kolton and A. Rosso, Spatiotemporal patterns in ultraslow domain wall creep dynamics, *Phys. Rev. Lett.*, 2017, **118**, 147208.
- 15 N. S. Deshpande, D. J. Furbish, P. E. Arratia and D. J. Jerolmack, The perpetual fragility of creeping hillslopes, *Nat. Commun.*, 2021, **12**, 3909.
- 16 N. S. Deshpande, P. E. Arratia and D. J. Jerolmack, *Athermal granular creep in a quenched sandpile*, *arXiv*, 2024, preprint, arXiv:2402.10338 [cond-mat.soft], DOI: [10.48550/arXiv.2402.10338](https://doi.org/10.48550/arXiv.2402.10338).
- 17 B. Ferdowsi, C. P. Ortiz and D. J. Jerolmack, Glassy dynamics of landscape evolution, *Proc. Natl. Acad. Sci. U. S. A.*, 2018, **115**, 4827.
- 18 M. Houssais, C. P. Ortiz, D. J. Durian and D. J. Jerolmack, Onset of sediment transport is a continuous transition driven by fluid shear and granular creep, *Nat. Commun.*, 2015, **6**, 6527.
- 19 E. A. Jagla, Down-hill creep of a granular material under expansion/contraction cycles, *Soft Matter*, 2023, **19**, 9308.
- 20 R. Eyles and R. Ho, Soil creep on a humid tropical slope, *J. Trop. Geogr.*, 1970, **31**, 40.
- 21 R. W. Fleming and A. M. Johnson, Rates of seasonal creep of silty clay soil, *Q. J. Eng. Geol. Hydrogeol.*, 1975, **8**, 1.
- 22 N. Matsuoka, The relationship between frost heave and downslope soil movement: field measurements in the Japanese alps, *Permafrost Periglacial Process.*, 1998, **9**, 121.
- 23 A.-V. Auzet and B. Ambroise, Soil creep dynamics, soil moisture and temperature conditions on a forested slope in the granitic vosges mountains, france, *Earth Surf. Processes Landforms*, 1996, **21**, 531.
- 24 N. Bontemps, P. Lacroix, E. Larose, J. Jara and E. Taïpe, Rain and small earthquakes maintain a slowmoving landslide in a persistent critical state, *Nat. Commun.*, 2020, **11**, 780.

- 25 S. V. Ketov, Y. H. Sun, S. Nachum, Z. Lu, A. Checchi, A. R. Beraldin, H. Y. Bai, W. H. Wang, D. V. Louzguine-Luzgin, M. A. Carpenter and A. L. Greer, Rejuvenation of metallic glasses by non-affine thermal strain, *Nature*, 2015, **524**, 200.
- 26 T. Divoux, H. Gayvallet and J.-C. Géminard, Creep motion of a granular pile induced by thermal cycling, *Phys. Rev. Lett.*, 2008, **101**, 148303.
- 27 B. Percier, T. Divoux and N. Taberlet, Insights on the local dynamics induced by thermal cycling in granular matter, *Europhys. Lett.*, 2013, **104**, 24001.
- 28 C. Pastén, E. Castillo and S.-H. Chong, Thermomechanical ratcheting in soil–structure interfaces, *Acta Geotech.*, 2019, **14**, 1561.
- 29 J. B. Coulibaly, M. Shah and A. F. Rotta Loria, Thermal cycling effects on the structure and physical properties of granular materials, *Granular Matter*, 2020, **22**, 80.
- 30 A. F. Rotta Loria and J. B. Coulibaly, Thermally induced deformation of soils: A critical overview of phenomena, challenges and opportunities, *Geomech. Energy Environ.*, 2021, **25**, 100193.
- 31 Y. Pan, D. Seo, M. Rivers, X. Gong, G. Buscarnera and A. F. Rotta Loria, Microscopic insights into thermal cycling effects in granular materials via x-ray microtomography, *Granular Matter*, 2024, **26**, 98.
- 32 Y. Pan, X. Gong and A. F. Rotta Loria, Thermal shakedown in granular materials with irregular particle shapes, *Sci. Rep.*, 2024, **14**, 6828.
- 33 H. N. Moseley, I. on the descent of glaciers, *Proc. R. Soc. London*, 1856, **7**, 333.
- 34 J. G. Croll, Thermally induced pulsatile motion of solids, *Proc. R. Soc. A*, 2009, **465**, 791.
- 35 B. Blanc, L. A. Pugnaloni and J.-C. Géminard, Creep motion of a model frictional system, *Phys. Rev. E: Stat., Nonlinear, Soft Matter Phys.*, 2011, **84**, 061303.
- 36 For this simple argument we assume static and dynamic friction forces to be equal.
- 37 I. Fernández Aguirre and E. A. Jagla, Critical exponents of the yielding transition of amorphous solids, *Phys. Rev. E*, 2018, **98**, 013002.
- 38 E. E. Ferrero and E. A. Jagla, Elastic interfaces on disordered substrates: From mean-field depinning to yielding, *Phys. Rev. Lett.*, 2019, **123**, 218002.
- 39 C. Liu, E. E. Ferrero, E. A. Jagla, K. Martens, A. Rosso and L. Talon, The fate of shear-oscillated amorphous solids, *J. Chem. Phys.*, 2022, **156**, 104902.
- 40 D. S. Fisher, Collective transport in random media: from superconductors to earthquakes, *Phys. Rep.*, 1998, **301**, 113, cond-mat/9711179.
- 41 M. Kardar, Nonequilibrium dynamics of interfaces and lines, *Phys. Rep.*, 1998, **301**, 85.
- 42 S. Bustingorry, A. B. Kolton and T. Giamarchi, Thermal rounding of the depinning transition, *EPL*, 2007, **81**, 26005.
- 43 E. E. Ferrero, S. Bustingorry, A. B. Kolton and A. Rosso, Numerical approaches on driven elastic interfaces in random media, *C. R. Phys.*, 2013, **14**, 641.
- 44 A. B. Kolton and E. A. Jagla, Thermally rounded depinning of an elastic interface on a washboard potential, *Phys. Rev. E*, 2020, **102**, 052120.
- 45 A. B. Kolton, A. Rosso, T. Giamarchi and W. Krauth, Dynamics below the depinning threshold in disordered elastic systems, *Phys. Rev. Lett.*, 2006, **97**, 057001.
- 46 In yielding under applied stress there is a problem similar to the one that distinguish static from dynamic friction. If a system is well annealed, applying a stress slightly above σ_c would not be sufficient to set it in ‘motion’ (plastic flow) but once it’s flowing it will flow as soon as $\sigma > \sigma_c$ is maintained. σ_c in our framework is the dynamical yield stress.
- 47 E. E. Ferrero and E. A. Jagla, Criticality in elastoplastic models of amorphous solids with stress-dependent yielding rates, *Soft Matter*, 2019, **15**, 9041.
- 48 P. Hébraud and F. Lequeux, Mode-Coupling Theory for the Pasty Rheology of Soft Glassy Materials, *Phys. Rev. Lett.*, 1998, **81**, 2934.
- 49 E. Agoritsas and K. Martens, Non-trivial rheological exponents in sheared yield stress fluids, *Soft Matter*, 2017, **13**, 4653.
- 50 Although we haven’t performed a systematic finite size analysis of σ_c in this occasion, we have checked that for a given system size N the values we can infer from a log-lin version of Fig. 3 for each k are consistent with the hand-tuned values that give a good power-law in the inset. Furthermore, the difference of $\sigma_c(L)$ between $L = 128$ and $L = 1024$ is smaller than a 2%.
- 51 H. Leschhorn, Interface depinning in a disordered medium—numerical results, *Phys. A*, 1993, **195**, 324.
- 52 D. S. Fisher, Collective transport in random media: from superconductors to earthquakes, *Phys. Rep.*, 1998, **301**, 113.
- 53 Yet, reaching the true steady state for each value of f is not equally easy when coming from below f_c increasing f and when starting from $f \gg f_c$ and decreasing it. We check consistency by simulating both protocols and with this we estimate an uncertainty in f_c .
- 54 Let us also mention that in order to achieve convergence in the values of w obtained, a relatively large number of cycles in k must be performed at each value of f .
- 55 X. Cao, S. Bouzat, A. B. Kolton and A. Rosso, Localization of soft modes at the depinning transition, *Phys. Rev. E*, 2018, **97**, 022118.
- 56 For yielding in $d = 2$ dimensions, estimations of ν exist (e.g. $\nu \simeq 1.16^{70}$); so our result can be used to guess – through scaling arguments – the ‘roughness’ of the elastoplastic manifold at criticality. We leave this discussion for a future work.
- 57 E. J. Gabet, Gopher bioturbation: field evidence for non-linear hillslope diffusion, *Earth Surf. Processes Landforms*, 2000, **25**, 1419.
- 58 R. García-Rojo and H. J. Herrmann, Shakedown of unbound granular material, *Granular Matter*, 2005, **7**, 109.
- 59 Y. Yuan, Z. Zeng, Y. Xing, H. Yuan, S. Zhang, W. Kob and Y. Wang, From creep to flow: Granular materials under cyclic shear, *Nat. Commun.*, 2024, **15**, 3866.

- 60 M. Le Goff, E. Bertin and K. Martens, Criticality at a finite strain rate in fluidized soft glassy materials, *Phys. Rev. Lett.*, 2019, **123**, 108003.
- 61 A. Pons, A. Amon, T. Darnige, J. Crassous and E. Clément, Mechanical fluctuations suppress the threshold of soft-glassy solids: The secular drift scenario, *Phys. Rev. E: Stat., Nonlinear, Soft Matter Phys.*, 2015, **92**, 020201.
- 62 S. Suresh, *Fatigue of Materials*, Cambridge University Press, 2nd edn, 1998.
- 63 In service conditions, the progressive increase in crack length produces an increase in stress intensity factors at the crack tip that lead eventually to a catastrophic failure of the sample.
- 64 C. G. Robertson, R. Stoček and W. V. Mars, The fatigue threshold of rubber and its characterization using the cutting method, in *Fatigue Crack Growth in Rubber Materials: Experiments and Modelling*, ed. G. Heinrich, R. Kipscholl and R. Stoček, Springer International Publishing, Cham, 2021, pp. 57–83.
- 65 A. K. Bhowmick, Threshold fracture of elastomers, *J. Macromol. Sci., Part C: Polym. Rev.*, 1988, **28**, 339.
- 66 T. Gibaud, T. Divoux and S. Manneville, Nonlinear mechanics of colloidal gels: Creep, fatigue, and shear-induced yielding, in *Encyclopedia of Complexity and Systems Science*, ed. R. A. Meyers, Springer Berlin Heidelberg, Berlin, Heidelberg, 2020, pp. 1–24.
- 67 S. Pradhan, A. Hansen and B. K. Chakrabarti, Failure processes in elastic fiber bundles, *Rev. Mod. Phys.*, 2010, **82**, 499.
- 68 G. Gradenigo, E. E. Ferrero, E. Bertin and J.-L. Barrat, Edwards thermodynamics for a driven athermal system with dry friction, *Phys. Rev. Lett.*, 2015, **115**, 140601.
- 69 E. A. Jagla, The prandtl–tomlinson model of friction with stochastic driving, *J. Stat. Mech.: Theory Exp.*, 2018, **2018**, 013401.
- 70 J. Lin, E. Lerner, A. Rosso and M. Wyart, Scaling description of the yielding transition in soft amorphous solids at zero temperature, *Proc. Natl. Acad. Sci. U. S. A.*, 2014, **111**, 14382.